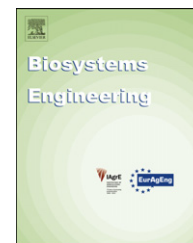Available online at www.sciencedirect.com

SciVerse ScienceDirect

journal homepage: www.elsevier.com/locate/issn/15375110

Research Paper

LiDAR simulation in modelled orchards to optimise the use of terrestrial laser scanners and derived vegetative measures

Valeriano Méndez [a,*], Heliodoro Catalán [a], Joan R. Rosell-Polo [b], Jaume Arnó [b], Ricardo Sanz [b]

[a] Department of Applied Mathematics, Polytechnic University of Madrid, Ciudad Universitaria, s/n, 28040 Madrid, Spain
[b] Department of Agricultural and Forest Engineering, University of Lleida, Rovira Roure, 191, 25198 Lleida, Spain

ARTICLE INFO

Light detection and ranging (LiDAR) technology is beginning to have an impact on agriculture. Canopy volume and/or fruit tree leaf area can be estimated using terrestrial laser sensors based on this technology. However, the use of these devices may have different options depending on the resolution and scanning mode. As a consequence, data accuracy and LiDAR derived parameters are affected by sensor configuration, and may vary according to vegetative characteristics of tree crops. Given this scenario, users and suppliers of these devices need to know how to use the sensor in each case. This paper presents a computer program to determine the best configuration, allowing simulation and evaluation of different LiDAR configurations in various tree structures (or training systems). The ultimate goal is to optimise the use of laser scanners in field operations. The software presented generates a virtual orchard, and then allows the scanning simulation with a laser sensor. Trees are created using a hidden Markov tree (HMT) model. Varying the foliar structure of the orchard the LiDAR simulation was applied to twenty different artificially created orchards with or without leaves from two positions (lateral and zenith). To validate the laser sensor configuration, leaf surface of simulated trees was compared with the parameters obtained by LiDAR measurements: the impacted leaf area, the impacted total area (leaves and wood), and the impacted area in the three outer layers of leaves.

© 2013 IAgrE. Published by Elsevier Ltd. All rights reserved.

1. Introduction

The contactless and non-destructive geometrical and structural characterisation of plants has been a subject of research both in forest and agriculture over recent years, with the use of light detection and ranging (LiDAR) in agriculture being a relatively more recent development. This interest is due to the fact that many fundamental properties and environmental interactions of plants and crops are related to the geometrical structure of their main components. In this context, several sensing techniques have been developed while others are the subject of continued research. Of the latter, stereo vision and LiDAR laser scanners are the most promising and complementary techniques from an operational and practical use and from a real field conditions point of view (Rosell & Sanz, 2012).

LiDAR is an increasingly used optical active remote sensing technique that measures range and/or other information of a

---

Nomenclature

+	Branching morphologic function. A shoot in a new axis is created by sympodial bud growth.
>	Succession morphologic function. A new shoot is created by apical bud growth.
α	Angle used in a turn geometric operation (degrees).
β	Polar angle used in shady process (degrees).
$\mathbf{d}, \mathbf{d}_2$	A direction in a vertex used for apical or sympodial growth.
$\Delta\theta$	Angle increase between two different laser beams (°).
Δy	Distance increase in the advance of the tractor (mm).
F	Floral state, which results from floral differentiation of the apical meristem
GU	Growth unit.
I_{3L}	3-external impacted leaf area (dm^2).
I_L	Impacted leaf area (dm^2).
I_T	Impacted total area (dm^2).
φ	Azimuth angle used in shady process (°).
L	Long state composed in general of 20 metamers.
L_A	Foliar area (dm^2).
l_{ij}	Measured distance (mm) where $i = 1, …, N$ and $j = 1, …, M$, given that N is the number of different laser beams and M is the number of steps in the tractor route.
M	Medium state composed in general of 8 metamers.
Ni	Number of internodes.
$\mathbf{n}$	A normal direction used in a turn geometric operation.
O	A point at the end of a branch where a bud is located, and where a geometric turn is calculated to get a new branching direction.
P	A position of the scan sensor from which a laser beam starts.
p_{ij}	Markov probability matrix.
θ	Angle of a particular sampling beam in the scan, separated by $\Delta\theta$ from the previous laser beam (°).
R	Lindenmayer's system production.
$\rho(u)$	A parent vertex in a Markov tree.
S	Short state composed of a single metamer.
Ta	Tree age.
u	A vertex in a Markov tree.
Ω	The alphabet of the L-system.
w	Initial axiom in an L-system.
x	The lateral distance from the scanner positioned in the inter-row (mm).
x_0	The distance from the laser to the orchard (mm).
y	Cross-sectional advance in the OY axis (mm).
z	Height coordinates in the model (mm).
z_0	The height of the laser above the ground (mm).

distant target. For this purpose, LiDAR systems (LS) comprise a laser emitter, which sends a light beam that strikes the object of interest, and a light detector that captures a portion of the radiation reflected by the object. By means of electronically processing of the target's scattered light, LS can determine the distance between the sensor and the object. Two different principles can be used for the measurement of range: i) the measurement of the phase-shift between the emitted and the reflected laser beam (Phase-shift LiDAR), and ii) the measurement of the time elapsed between the emission of a laser pulse and its detection after being scattered by the target (Time-of-flight LiDAR). Most LS usually work in scanning mode, changing the light emitting direction within a plane thousands of times per second and measuring the distance for each angular direction with great precision. The measurement outputs are usually the three-dimensional (x, y, z) spatial coordinates of each detected point (so-called point clouds) although some LS provide other measurements such as the intensity of one or more reflected laser beams. The use of appropriate post-processing algorithms makes it possible to describe and reconstruct the structure of the trees with a high degree of accuracy (Rosell, Llorens, et al., 2009).

Many studies have focused on exploring the application of LS to characterise both forest canopies (Holmgren & Persson, 2004; Lefsky et al., 1999; Maltamo, Eerikäinen, Pitkänen, Hyyppä, & Vehmas, 2004; Omasa, Hosoi, & Konishi, 2007; Parker, Harding, & Berger, 2004; Riaño, Chuvieco, Condés, González-Matesanz, & Ustin, 2004), and agricultural crops. As regards the latter, the evaluation of vegetative parameters

both in tree crops (Tumbo, Salyani, Whitney, Wheaton, & Miller, 2002; Wei & Salyani, 2005) and in herbaceous crops (Ehlert, Heisig, & Adamek, 2010; Gebbers, Ehlert, & Adamek, 2011; Saeys, Lenaerts, Craessaerts, & De Baerdemaeker, 2009), the obtaining of 3-D structure of trees (Rosell, Llorens, et al., 2009), and the estimation of leaf area in fruit trees and vineyards (Arnó et al., 2012; Palacín et al., 2007; Rosell, Sanz, et al., 2009) are among the most relevant application areas of interest.

Also, the application of plant protection products (PPP) in tree crops has recently opened the opportunity for the application of different sensors and electronic control devices on sprayers. For instance, through the use of ultrasonic sensors it is possible to apply pesticide treatments distinguishing the presence or absence of trees. If in addition a device that allows an online calculation of leaf area or volume for each tree detected is incorporated to this technique, it is possible not only to apply in the right places, but also vary dose with foliar area or volume (Gil, Escolà, Rosell, Planas, & Val, 2007; Solanelles et al., 2006). However, although ultrasonic sensors allow variable application dosage adapted to the canopy characteristics, the use of LiDAR sensors presents advantages given their higher spatial resolution and measuring speed (Escolà et al., 2007; Llorens, Gil, Llop, & Escolà, 2011). In fact, in research studies related to the optimisation of pesticide treatments, Walklate, Richardson, Baker, Richards, and Cross (1997, 2002) introduced a methodology to calculate several geometrical parameters in apple trees based on the possibilities offered by LS. These authors obtained their results

through a probabilistic interpretation of the interaction of the light emitted by the sensor with the plants.

Concerning the construction of virtual vegetation, the first method used to create sophisticated plant topology was that of modular representation. Plants develop as repetitions of certain types of components (Barthélémy, Edelin, & Halle, 1991; Bell, 1994; Harper, Rosen, & White, 1986). A modular representation can be developed using spatial, geometrical or topological approaches. In geometric modular representation, plants are decomposed in organs as leaves, fruits or internodes. This type of representation enables a precise description of the plant to be obtained by studying the interaction between plants and their microenvironment (Dauzat, 1993; Sinoquet, Adam, Rivet, & Godin, 1998). Topologic modular representation is a decomposition in which emphasis is placed on the connections between organs. Several models of water flux in plants have been proposed based on an electrical analogy (Dauzat, Rapidel, & Berger, 1999; De Reffye, Fourcaud, Blaise, Barthélémy, & Houllier, 1997; Früh, 1997). The topologic model has been used to address carbon-partitioning problems. The modelling of pipes, where every pipe is related to a leaf, is an example of topologic model (Shinozaki, Yoda, Hozumi, & Kira, 1964; Valentine, 1985). As computer calculation capacity has expanded, plant growing simulation programs which utilise the topologic model have been used to develop realistic three-dimensional models of the plant architecture (Diggle, 1988; Fisher & Weeks, 1985; Ford, Avery, & Ford, 1990; Prusinkiewicz & Lindenmayer, 1990; Weber & Penn, 1995). Classical modular representations have been completed based on systems of branch, axis and different types of growth units (GUs) or internodes. In addition to this, a statistical approach, illustrated by Guédon, Barthélémy, Caraglio, and Costes (2001), has become essential for the analysis of architectural data. The statistical framework of the hidden Markov tree (HMT) model was introduced by Crouse, Nowak, and Baraniuk (1998) for modelling a tree-structured process. Markovian models for tree-structured data have been integrated into the AMAPmod software (Godin, Guédon, Costes, & Caraglio, 1997).

Therefore, there are to date several methods for generating virtual trees and in particular fruit trees. On the other hand, recent research has demonstrated the benefits of LS as crop sensors and their application in different areas. However, doubts arise when considering how to use these devices in field conditions or, as it is called, in a real LiDAR system operation (LSO). In this regard, many field tests would be unnecessary if simulators of LiDAR operation in virtual orchards could be available. Assuming virtual trees are close to reality, LiDAR system simulators (LSSs) can be used to optimise the configuration of LSO for the estimation of canopy volumes and tree foliage surfaces for different precision agricultural practices as plant protection, fertilisation and precise irrigation (Garrido et al., 2012). Other possible application could be the simulation of light distribution within the canopies given its influence on crop growth and yield. Estimation of shaded area by the canopy is also gaining relevance due to its relation with precision irrigation scheduling and water demand of crops. Finally, evaluating virtual trees (or tree models) can be performed using the LSS as validation. In fact, the LSS would allow testing of the sensibility of parameters obtained in a real

LSO survey by performing different virtual processes in creating trees. As suggested by Delagrange and Rochon (2011), the idea being to verify which growth-pattern allows a virtual tree close to the original tree. Once validated, the virtual tree can substitute the need of manual defoliation to measure the leaf area index (LAI), among other parameters.

To sum up, LSS programs would allow the processes of growth and vegetative characteristics for virtual trees to be investigated. In this regard, the aim of this study is to develop simulation software to obtain fruit trees and the subsequent operation of a virtual LiDAR sensor or LSS. The trees should be able to include both ligneous and orchard's foliar structure. The subsequent validation consists in comparing the simulated characteristics of trees with the parameters obtained with the LSS. Ultimately, it is intended that researchers and users of LS will have a useful tool for configuring terrestrial laser sensors in real operations (LSO).

2. Materials and methods

The software presented here is an application developed in C++ that improves an early version (SIMLiDAR, Méndez et al., 2012). Firstly, the user can generate a virtual orchard (or canopy geometry) using a Lindenmayer, L-system, (Tarquis & González-Andrés, 1995; Tarquis, Méndez, Walklate, Castellanos, & Morató, 2006), or a Hidden Markov Tree modelling process, HMT (Costes et al., 2008; Durand, Guédon, Caraglio, & Costes, 2005). The generated tree depends on different plant parameters (number of reiterations, transition probabilities, phyllotaxis angle), being possible with this new version providing an own site with a three-dimensional scene based on OpenGL™ (http://www.opengl.org).

After obtaining the virtual tree, the program allows the simulation of a terrestrial laser scanner (LSS), and then determining some vegetative parameters from this simulation. Concerning data from the LSS, the program provides a set with the distances from laser beam origin to nearby plant objects (branches or leaves). The current work is focused on the estimation of actual foliar surface from parameters obtained using beam impacts. A method that correlates several impacted areas in a real laser operation (LSO) and leaf area (virtual orchard) was considered.

2.1. An improved hidden Markov tree (HMT) model for artificial orchards

The plant architecture starts from the foliar development of the apical meristem (Bell, 1994) that can undergo an undefined (monopodial) or defined (sympodial) growth. The model of vegetative development stems from the combination of different types of axis with morphological characteristics as growth patterns, branching type, phyllotaxis or spatial orientation. The architectural unit of the plant depends on the type of axis and growth model used. Growth occurs with axis production already present in previous stages, known as the reiteration process. Reiteration is a mechanism that allows building of the crown in the majority of trees (Barthélémy et al., 1991). Analysis of the plant architecture enables a detailed quantitative analysis (Tourn, Barthélémy, & Grosfeld,

Table 1 – Transition probability matrix. The value at line i and column j represents the probability of a transition ($\rho(u)$) from state i to state j. States (u) L, M and S are characterised by a high, medium and low number of metamers per GU, respectively; F stands for presence of flowers. (From Durand et al., 2005, p. 818).

u (previous state)	Transition probability matrix $\rho(u)$ − next state			
	L	M	S	F
L	0.05	0.15	0.63	0.16
M	0.02	0.06	0.30	0.62
S	0.01	0.05	0.27	0.66
F	0.04	0.35	0.60	0.00

1999) that allows measurement of the growth in structural units (Blaise, Barczi, Jaeger, Dinouard, & de Reffye, 1998; Godin et al., 1997). These models describe the meristem development from stochastic processes (De Reffye, Elguero, & Costes, 1991). On the other hand, it is possible to extract a distribution of axes in different kinds of metamer sequences or GU from quantitative studies. The metamer sequence is assimilable to a set of mutually exclusive random states. Crouse et al. (1998) introduced a HMT to model homogeneous areas. The number of states is determined using stochastic criteria. Detailed studies of apple trees have been carried out over branching patterns in 1-year trunks (Costes & Guédon, 2002), and in the architectural development of 6-year old trees (Costes, Sinoquet, Kelner, & Godin, 2003) applying the HMT to plant architecture (Durand, Gonçalvès, & Guédon, 2004) and with a stochastic and biomechanical model (Costes et al., 2008).

In this work, the development of a virtual tree is based on a structure of axes that, by reiteration, is expanded with new metamers that transit into different states. The transition from one state to the next is regulated according to a stochastic process based on a probability matrix belonging to a first order Markov chain. Specifically, the stochastic summary presented by Durand et al. (2005) in a transition matrix of four states is used (Table 1). The states defined by Durand correspond to the macroscopic states used in the software MappleT (Costes et al., 2008). These four states are long, medium, short and floral (L, M, S, F). Each state contains an average number of metamers (20, 8, 1 and 3, respectively). Adjustments have been introduced to determine the number of metamers according to the order number and age of the axes (Costes et al., 2003). The results of the functions $Ni = 96.436 \, e^{-0.37 \cdot Ta}$ for trunks, and $Ni = 68.525 \, e^{-0.33 \cdot Ta}$ for long shoots are tabulated

in Table 2, where Ta is the tree age and Ni the number of internodes. The model adopted is developed with the following entities: axis, branch and leaf. The branches and leaves depend on the state (transition matrix) of the axes. In fact, a branch corresponds in our model to a GU that could be different depending on the axis state. In a particular transition, the previous and following states are evaluated to determine the existence of apical succession or sympodial branching. Apical succession only involves the creation of a shoot according to the new state of the axis. Each shoot is a succession of metamers (one internode and one leaf), with the number of metamers shown in Table 2 and leaves following phyllotaxis rules. However, if there is a sympodial branching, a new axis is created using a fixed branching angle (to 35°) over the current axis direction. Up to three new axes can be created if the new state accepts all internodes. If the new state is developed from a short state (S, single internode), only one axis is created in the branching process.

The tree is initiated with a long first state (L), which determines the initial probability of the Markov chain. So, the (L, M, S, F) probability vector is (1,0,0,0). To make possible both growth options (apical succession or sympodial branching), the model uses two basic morphological functions that control the plant growth, the succession (noted as >) and the branching (noted as +). Durand et al. (2005) propose the use of two probability matrices to control both processes separately, although it is usual to use rules to control succession (>) and branching (+) depending on previous and following states (Costes et al., 2003, 2008; Durand et al., 2005). Moreover, straight axes are used because biomechanical correction to introduce tropism effects has not been considered (as is done by Costes et al., 2008). During a transition every axis is evaluated. To do this, the axis probability P^k is considered, P being the probability matrix proposed in Table 1 and k the number of transitions occurred in this axis. For instance, if a u vertex is in S_u state, the transition probability will be defined by a matrix $P = (p_{ij})$, where $p_{ij} = P(S_u = j | S_\rho(u) = i)$ represents the probability of a change from the i-th state in the $\rho(u)$ parent vertex to the state j in the u vertex (Fig. 1).

Table 2 – Number of internodes used per state, order of the axis and birth year.

State	Order	Year	Internodes
L	1	1	30
L	1	2, 3	25
L	1	≥4	20
L	≥2	≥1	20
M	≥1	≥1	9
S	≥1	≥1	1
F	≥1	≥1	3

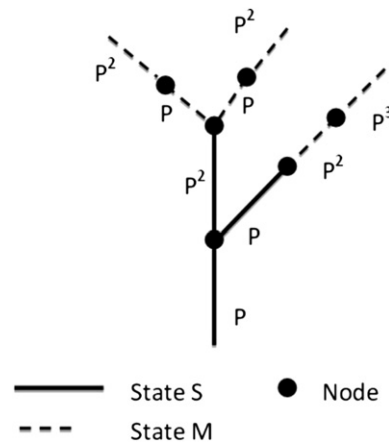|	
—— State S	● Node
- - - State M	

Fig. 1 – An example of the use of probability matrix P in succession & branching in different axes of the model for S and M state. A new power of P is used in succession. The original P is recovered in a new branching.

Each stage is formalised mathematically as follows. Given a unitary direction **d** from a point O, it is possible to obtain a new direction **d'** that has an α angle with the above mentioned rotation around point O. To do this, an intermediate normal direction **n** to a plane that contains the fixed point O and the direction **d** is required. Fig. 2 shows the procedure used to achieve this rotation. Specifically, the normal vector **n** is obtained by the vector product $\mathbf{n} = \mathbf{d} \times \mathbf{d_2}$, in which $\mathbf{d_2}$ is a direction not aligned to **d** and established arbitrarily. The application of Eq. (1) allows obtaining finally the new growth direction.

$$\mathbf{d'} = \cos\alpha \ \mathbf{d} + \sin\alpha \ (\mathbf{n} \times \mathbf{d}) + (1 - \cos\alpha)(\mathbf{n} \cdot \mathbf{d}) \ \mathbf{n} \qquad (1)$$

The arbitrary selection of $\mathbf{d_2}$ only has influence on the initial phyllotaxis angle which is applied to the first new branch in a current axis. Since there is no preference for the direction of

growth, the consecutive branches are turned **d'** from **d** (Fig. 2d) following a fixed phyllotaxis angle (set to 144° in the current work according to Costes et al., 2008). Thus, Eq. (1) changes to Eq. (2) using **d** instead of **n**, **d'** instead of **d**, and α taking values with phyllotaxis angle increments.

$$\mathbf{d''} = \cos\alpha \ \mathbf{d'} + \sin\alpha(\mathbf{d} \times \mathbf{d'}) + (1 - \cos\alpha)(\mathbf{d} \cdot \mathbf{d'})\mathbf{d} \qquad (2)$$

From experimental measurements of fruit tree canopies it was observed that the foliar distribution is greater in the outlying space, tending to maximise the solar exposure (Sanz et al., 2011). However, the foliar distribution within the canopy in the virtual model becomes thicker as the number of re-iterations increases. To reduce this effect, an algorithm that evaluates the shady index for each leaf is proposed. Thus, if the shady ratio reaches a threshold (model parameter), the
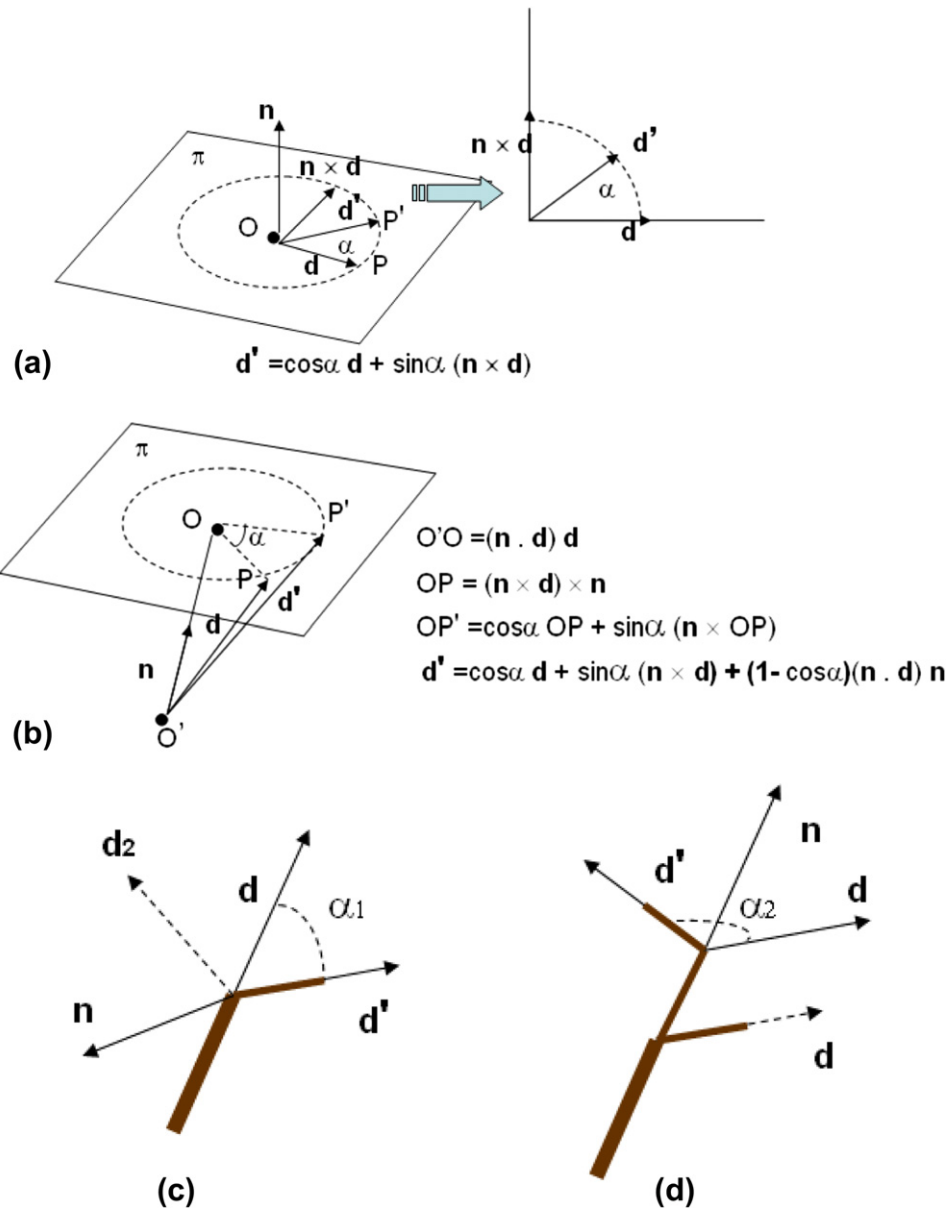

Fig. 2 — (a) Turning a vector d in the plane an angle α. (b) Turning a vector d in the space through a direction n an angle α. As a result of the turn a new vector d' is obtained (Scala, 1988). The turning (b) is applied to branching (c), where an arbitrary direction d_2 is taken to obtain n and a turn of α_1 is done. Subsequently, in the phyllotaxis turning (d), the direction n of turn is determined by the axis of the parent branch.

leaf is removed in the process of generating the virtual tree. Marking the centre of gravity of each leaf, the algorithm uses several semi-straights from this point to the infinity to search for any impact with other leaves. To get an acceptable processing time for this algorithm, the number of semi-straights must be necessarily limited. The semi-straights are selected according to a semi-spherical distribution in two directions β (polar angle) and ϕ (azimuth angle). The polar angle ranging between $[0°, 360°]$ and angular increments $\Delta\beta = 45°$ were used. In the case of the azimuth angle values were $[−90°, 90°]$ and $\Delta\phi = 15°$, respectively. The proposed method is independent of the shape of the tree canopy and does not require any type of data structure to support the calculation. Finally, the leaf area L_A for the virtual tree is measured as the sum of the individual areas of all the leaves of the orchard.

Figure. 3 (a) shows an example of the HMT apple tree model. To obtain this virtual orchard several parameters were used. Some parameters were previously fixed; the user can vary several others. However, the options considered were as follows.

- The dimension of the Markov model was set equal to 4. The probability matrix dimension and the number of different states depend on this parameter.
- The character strings that represent each state were L, M, S and F (Long, Medium, Short and Floral, respectively).
- The program operated on two probability matrices (one for succession and another for branching). Both were set to the same values according to Table 1.

- The branching angle was 35°.
- The phyllotaxis angle was 144°.
- The program allows the maximum number of new branches that can be obtained from the parent GU in the branching process to be set.
- Initial GU and initial direction were set to L state and (1,0,0) vector direction. Both define the first axis of the plant before starting the reiteration process.
- The internode length was 35 mm.
- The number of internodes used by state, axis order and birth year were set according to the values in Table 2.
- Branching and succession rules were established by parent-child state according to Table 3.

2.1.1. Other kinds of models

The new model presented in this paper continues to support the L-System model developed by Méndez et al. (2012). Thus, it is also possible to upload a virtual tree generated by an external tool provided that there is an interface for branches and leaves based on text files. For the branches, it is necessary to know the (x, y, z) coordinates from both the ends of the branch and the value of the diameter. For the leaves (x, y, z) coordinates of the leaf external polygonal chain or polyline must be known.

A Lindenmayer system (L-system) (Lindenmayer, 1968) builds complex objects, as a branching pattern of a tree, by successively replacing parts of an initial object using a set of
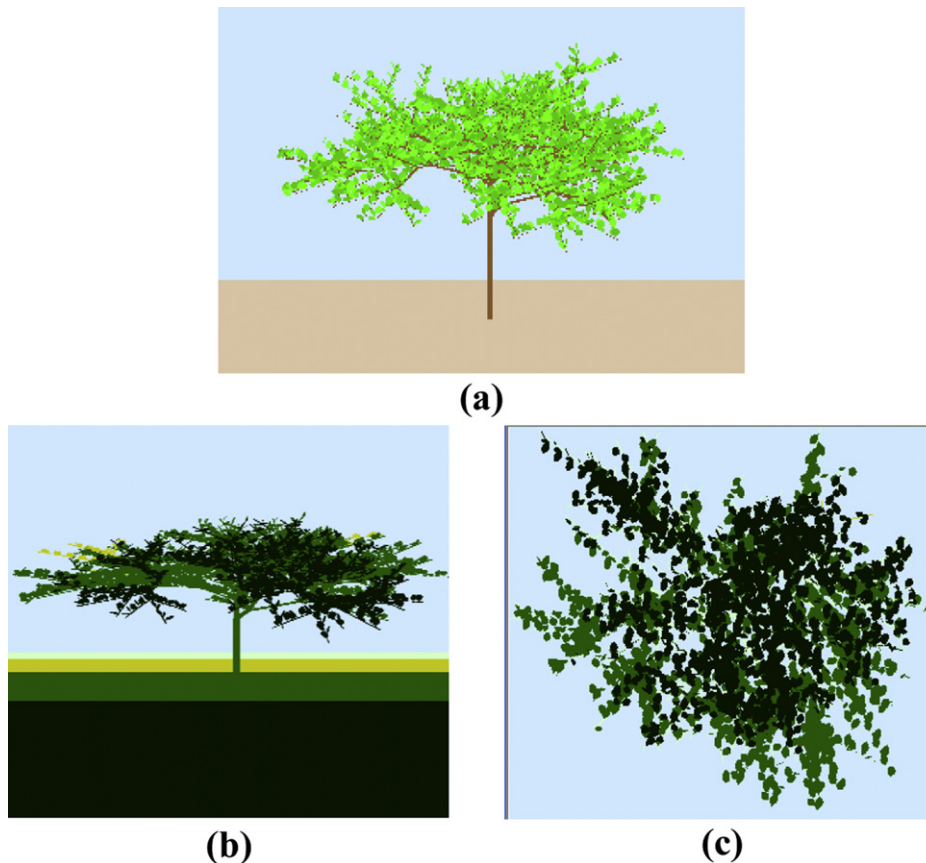

(a)

(b)

(c)

Fig. 3 − An example of a three-dimensional HTM model for apple trees with a number of reiterations equal to 10 and a shady percentage of 80%. (a) view of virtual apple tree. (b) lateral angular scan. (c) zenith scan.

Table 3 — Succession and branching existence per parent-child state (see Fig. 5 in Durand et al., 2005, p 820).

Parent	Child	Succession	Branching
L	L	Yes	Yes
L	M	Yes	
L	S		Yes
L	F	Yes	
M	L		
M	M	Yes	
M	S		Yes
M	F	Yes	Yes
S	L		
S	M		
S	S		Yes
S	F	Yes	
F	L		
F	M		Yes
F	S		Yes
F	F		

rewriting rules or productions (R). The rewriting rules, proposed by Von Koch (1905) operate on character strings, or alphabet (Ω), as a formal grammar (Chomsky, 1956). The rewriting process starts from a distinguished string, called the axiom (w) that represents a budding tree. In each iterative step the active bud is replaced by a new branch structure so, for example, active buds and branches are letters of the alphabet. Prusinkiewicz and Lindenmayer (1990) define a deterministic L-system as a triplet {Ω, w, R}, where Ω is the alphabet, w the axiom and R the productions set. The process has two stages; in the first a string substitution is carried out from the initial string (w) replacing a letter by a new substring according to production rules (R). Every symbol is replaced in the string as many times as it appears. At the end of the first stage a final string is obtained, which is interpreted according to turtle geometry (Abelson & di Sessa, 1982). A turtle is an intrinsic geometry that can be assimilated to a drawing cursor in 3D, with two parameters (position and orientation) that describe the virtual plant modelling.

2.2. Simulation of the laser sensor

The virtual tractor-mounted LiDAR advances along the row (OY axis), and the laser beam is directed towards the interior of the vegetation (OX axis). Through a secondary angular movement in the XZ plane the scanner measures the distances to the virtual orchard, as shown in Méndez et al. (2012) for ligneous models. In the current work, leaves are included in the model resolving the scan simulation with two basic movements. The main movement (y) is a cross-sectional advance along the OY axis from a starting point y_1, carrying out successive incremental advances of Δy (simulation parameter). A secondary angular movement (θ) takes place between two fixed angular values (θ_{min} and θ_{max}) at a given position of the OY axis (y_i). Thus, the laser beam advances incrementally by Δθ, which is also a parameter in the program. In each displacement of y_i, angles θ_{min} and θ_{max} are calculated from the laser sensor position and the maximum plant height. Finally, at each position of the laser beam (y_i, θ_k), a search is

performed for the impacts between the virtual laser beam and the leaves of the modelled tree.

The set of impacts between leaves and laser beams is found by solving a straight line/plane intersection problem because the leaves are modelled by plane closed polygons. The branches/laser beam intersection is quite different. The end of the laser beam is modelled as a small three-dimensional mesh and an intersection is considered when some point of the mesh is inner to the branch trunk cylinder (Méndez et al., 2012). If the laser beam is not intercepted by the tree, it may be intercepted by the ground (when $\theta < 0$) or, in some cases, it may not be intercepted at all (when $\theta > 0$). In the first case the distance to the ground is recorded, while in the second case an escape distance is recorded (in fact, a constant is used with a distance much greater than any possible interception). The result of the simulation is a matrix L where each $l_{i,k}$ element is the laser beam distance from LiDAR to the tree model in each (y_i, θ_k) laser position. In matrix L $i = 1, …, N$ is the number of different laser beams depending on the resolution used, and $k = 1, …, M$, is the number of increments (Δy) along the tractor route.

The LiDAR simulation (LSS) is done through lateral measurements from one side of the tree. The lateral operation of LiDAR from the opposite side is also included in the simulation. It could be established an internal coordinated reference that links both processes, because each row is related with a y value of cross-section advance. In any case, it is sufficient to simulate only one side of the vegetation for estimating the leaf area and other vegetative parameters. Moreover, a third option may be used in the simulation of the scanning process. Specifically, a new zenith position of LiDAR is included, assuming that the scanning is carried out overhead at a sufficient height (simulating an aerial scan). Besides all this, the program can perform angular (default) and also orthogonal scanning. The latter could only be applied when the distance of the laser to tree is very large (for example, overhead), or to simulate several lasers mounted in a vertical bar. In this case, the laser beams are projected parallel to the OX axis, so the system records the distances from the LiDAR to the parallel YZ planes resulting from different intercepts (Fig. 4). The program also permits virtual scanning on two rows, getting different random trees in both. In such cases a specific simulation operates by moving the tractor in the middle of the two rows. The result is two files for the scan of each side, left or right.

To detect the impacts, a scanner position P = (x y z) is assumed (Fig. 5). When an impact occurs, the intercept point (**R**) must belong to the straight line R = P + t·**d**   (t∈ℜ), with **d** being the unitary direction of the laser beam. When the polyline of a leaf containing the point Q and following an orthogonal direction w impacts with the laser beam occurs, the expression t = ±(P − Q)·**w/d**·**w** will be true, with R being an inner point of the leaf (Fig. 5). The values of P and **d** will depend on the type of scan selected in Table 4. The interception between the laser beam and the ligneous structure is solved according to the criteria of Méndez et al. (2012). Thus, the interception between the laser beam and a branch is calculated using a dot matrix. A set of points are evaluated to determine if they are inner to a cylindrical trunk object, and then it is decided whether the laser beam does or does not intercept a branch.
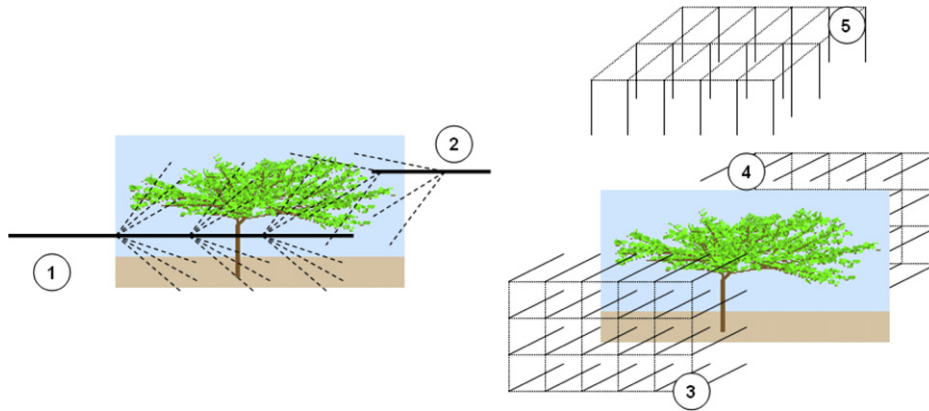
Fig. 4 − Type of scan. Lateral angular (1), opposite lateral angular (2), orthogonal lateral (3), opposite orthogonal lateral (4) and zenith (5).

2.2.1. Leaf area and tree measurements

A standard LiDAR operation obtains a matrix of the distances measured. Every distance is related with an angular position of the laser beam and an average angular and cross-advance increase can be considered for all the operation. All previous data allow a discrete impacted area for each laser beam to be estimated, being the sum of all the impacted total area (I_T) of a LiDAR operation. The program could measure I_T in this manner. However, as the program has established which objects are branches or leaves, it can also differentiate which impacts occur at a leaf object and sums them, thus obtaining the impacted leaf area (I_L). Moreover, when the program finds an impact with a leaf, it extends the direction of the laser

beam to count secondary intersections with other leaves behind the first one. It sums these discrete areas into the so-called impacted area in the three outer layers of leaves (I_{3L}). The extension of the laser beam direction founding secondary leaves stops if a branch object is found. In the virtual model the leaves and wood objects are typified to distinguish easily where the impact has occurred. This does not happen in a real LiDAR operation. Since the virtual leaf area (L_A) is known, a regression analysis may be performed to predict L_A using the parameters of LiDAR simulation (I_T, I_L and I_{3L}). In any case, the regression analysis is used as LiDAR validation procedure.

#### 2.2.2. Formulae used in the model

When a laser beam hits a branch or leaf, the impacted total area is considered to be the projection on the YZ plane obtained by the following equation:

$$\Delta y \cdot \left[\left(z_0 + l_{ij} \cdot \sin\left(\theta_j + \Delta\theta \right) \right) - \left(z_0 + l_{ij} \cdot \sin\theta_j \right) \right] \tag{3}$$

where z_0 is the height of the laser above the ground, and l_{ij} and θ_j are the distance and the impact angle, respectively. As such, the total detected (impacted) area will be equal to

$$I_T = \sum_{i,j} \Delta y \cdot \left[\left(z_0 + l_{ij} \cdot \sin\left(\theta_j + \Delta\theta \right) \right) - \left(z_0 + l_{ij} \cdot \sin\theta_j \right) \right] \tag{4}$$

The impacted leaf area (I_L) is obtained considering only the impacts on leaves and also using Eqs. (3) and (4). However, the impacted area in the three outer leaves (I_{3L}) is different as it is obtained by applying Eqs. (3) and (4) up to a maximum of the
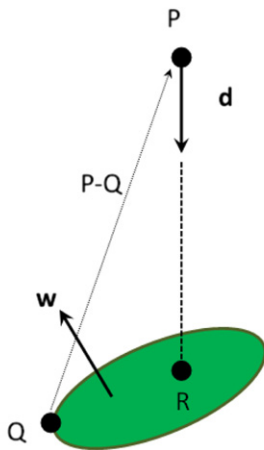
(P-Q).**w** : Distance from P to leaf plane

d.w : Modulus of **d** projected over **w**

$\dfrac{(P-Q).\mathbf{w}}{\mathbf{d.w}}$: Scale to use in **d** to impact in leaf plane

Fig. 5 − Calculation of impact (R) of one laser beam in a leaf. P is the scanner origin and Q is an arbitrary point of a polyline that contains the leaf.

Table 4 − Laser beam starting point (P) and laser beam direction (d) by type of scan. (x_0, y_0, z_0) is the scanner position which is fixed in all the scanning process.

Type of scan	P	d
Lateral and angular	(x_0, y_i, z_0)	($\cos\theta_k$, 0, $\sin\theta_k$)
Opposite lateral and angular	(x_0, y_i, z_0)	($\cos\theta_k$, 0, $\sin\theta_k$)
Lateral and orthogonal	(x_0, y_i, z_i)	(−1, 0, 0)
Opposite lateral and orthogonal	(x_0, y_i, z_i)	(1, 0, 0)
Zenital (orthogonal)	(x_i, y_i, z_0)	(0, 0, −1)

first three leaves (or layers) in the tree, provided that no woody structure is intercepted before (Fig. 6). Therefore, it is expected that intuitively the magnitude of the three impacted areas may be ordered as $I_L < I_T < I_{3L}$. These areas are then used as regressor variables to predict the leaf area (L_A) of simulated apple trees.

2.3. Tests to evaluate the simulation program

Twenty different virtual orchards were obtained by the HMT model. The number of iterations in the process and the shady index were varied to obtain apple trees with different structure and geometry. Specifically, orchards were obtained after applying 7, 8, 9, 10 or 11 iterations. The shady percentages were 60, 70, 80 and 101 (the latter indicated that no shading was considered and no leaves were removed at the end of the simulation process). Concerning the LiDAR simulation, two scanning processes were performed, according to the sensor position and the laser beam projection. First, the sensor was simulated in lateral position and projecting the beam angularly with respect to the row. In the other case, the sensor was simulated in zenith position and orthogonal projection of the beam. In terms of formulae, the horizontal resolution (or cross-sectional increment) was set to $\Delta y = 0.002$ m. An angular resolution of $\Delta\theta = 0.25°$ was used when the beam was simulated with angular projection.
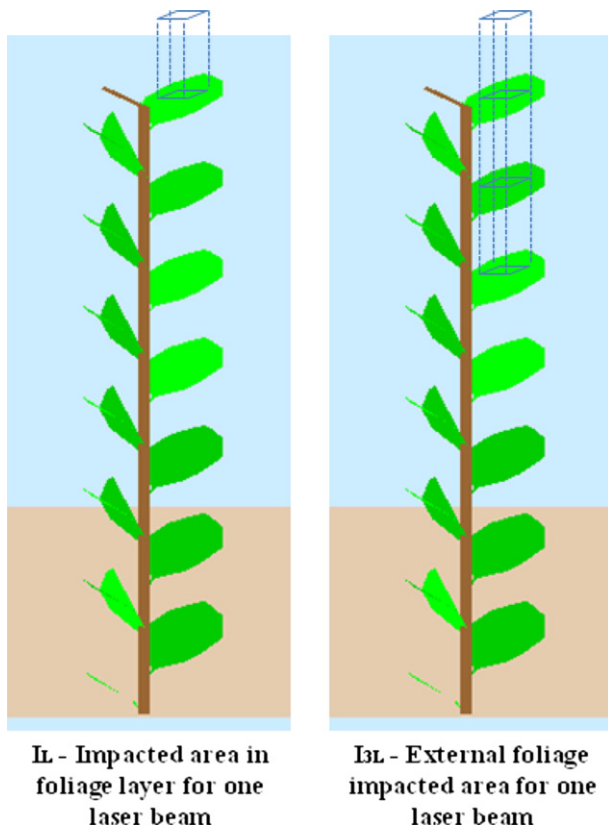

I_L - Impacted area in foliage layer for one laser beam

I_{3L} - External foliage impacted area for one laser beam

Fig. 6 − An example of a unitary laser beam of I_L − impacted area in foliar layer and I_{3L} − external foliar impacted area. The impacted area (I_T) is equivalent to I_L whether the impacted model object is a leaf or a branch.

3. Results and discussion

The LiDAR sensor simulation developed here reported some interesting results. As intended, the LSS has allowed to evaluate the performance of a LiDAR sensor in real operating conditions (LSO) using in this case virtual apple trees. The first consideration to note is that the sensor may have different behaviour depending on the mode of use. There was a very satisfactory estimate of tree leaf area (L_A) when the LiDAR sensor was used from the side of the row (which is the normal position of use). However, the use of the sensor from an elevated position, above the row, slightly improved the previous results. The reasons for this effect are unclear. However, some discussion could be made on the basis of the regression models obtained. Overall, a good linear correlation was found between the aforementioned leaf area of virtual trees (L_A) and the impacted areas using the LiDAR (I_L, I_T, and I_{3L}) (Fig. 7).

For the lateral scanning process Eqs. (5)−(7) show different behaviour near the origin. In fact, only the model that computed all impacts (i.e. leaves and wood) presented an intercept. This was an expected result, since with leafless trees the impacted area will always be greater than zero due to the presence of branches. This effect also occurs in the zenith scan.

$$L_A = 12.67 \cdot I_L \quad (R^2 = 0.95) \tag{5}$$

$$L_A = 8.70 \cdot I_T - 209.15 \quad (R^2 = 0.94) \tag{6}$$

$$L_A = 6.40 \cdot I_{3L} \quad (R^2 = 0.97) \tag{7}$$

Another interesting effect is the value of the regression coefficients. Given that impacted leaf area (I_L) was lower than impacted total area (I_T), the regression analysis gave a higher regression coefficient (12.67) for the regressor variable I_L in comparison with I_T (8.70). The lowest regression coefficient (6.40) corresponded to the variable I_{3L} which was expected since the surface impacted in the first three leaves is greater than in others. The same trend has occurred when the sensor scanned from overhead. Eqs. (8)−(10) were obtained for this case.

$$L_A = 7.10 \cdot I_L \quad (R^2 = 0.97) \tag{8}$$

$$L_A = 6.71 \cdot I_T - 129.84 \quad (R^2 = 0.96) \tag{9}$$

$$L_A = 3.29 \cdot I_{3L} \quad (R^2 = 0.99) \tag{10}$$

Comparing both procedures it was noted that zenith scans always provided regression coefficients lower than the corresponding lateral equations. This may be due to the growth pattern and training system of the simulated tree structure. Using LiDAR measurements Sanz et al. (2011) have shown that trees tend to grow laterally by opening the canopy for a better use of sunlight. More specifically, leaves tend to grow outward from the canopy for light for photosynthesis. This probably causes an increased foliar exposure from an overhead view as opposed to a lateral one, which is more obvious when the open vase form was adopted as the growth pattern (or training system) in the HMT modelling. Therefore, it is not surprising
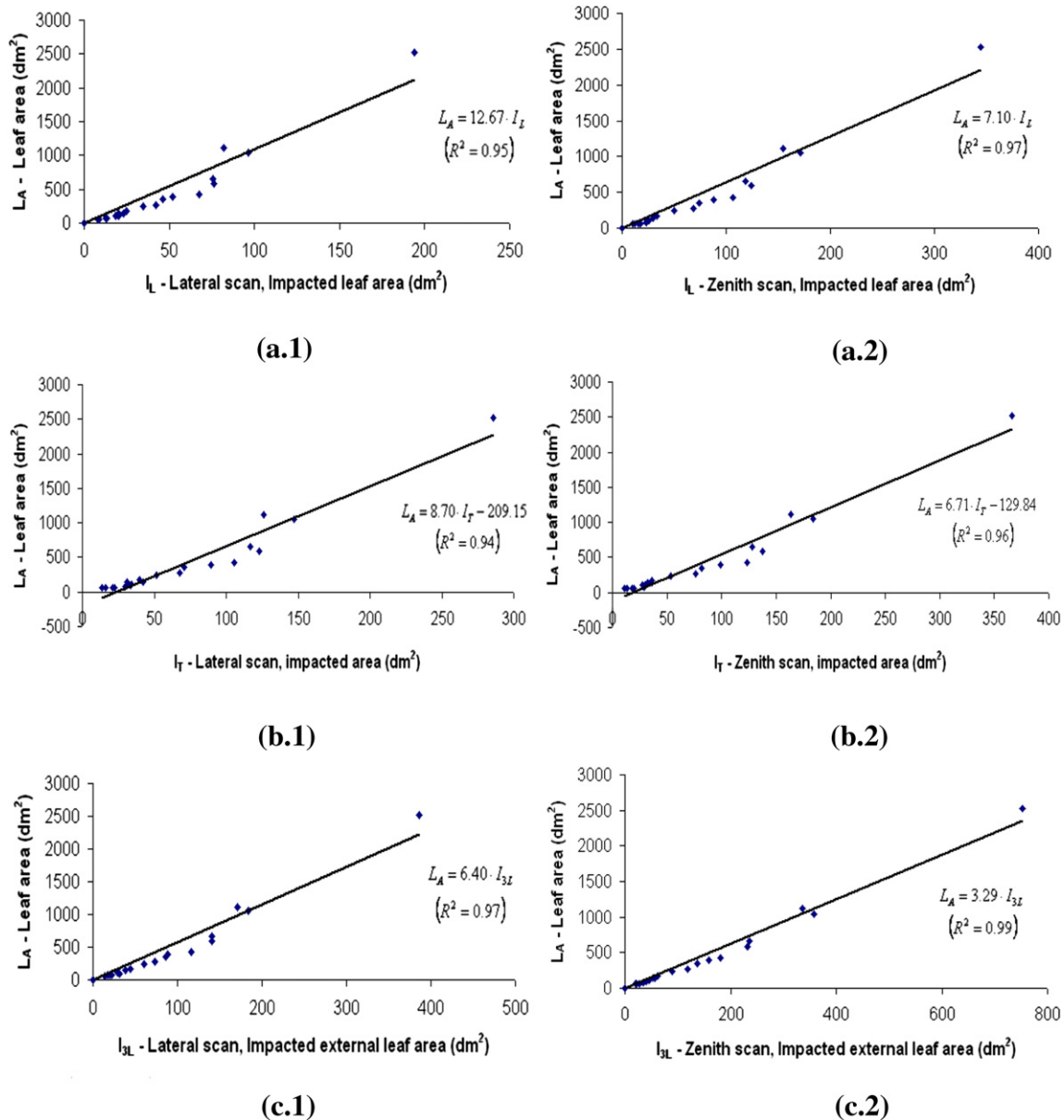
Fig. 7 − (A) L_A − leaf area (dm^2) vs. I_L − impacted leaf area (dm^2). For lateral scan $L_A = 12.67 \cdot I_L$ with $R^2 = 0.95$ (a.1). For zenith scan $L_A = 7.10 \cdot I_L$ with $R^2 = 0.97$ (a.2). (b) L_A − leaf area (dm^2) vs. I_T − impacted area (dm^2). For lateral scan $L_A = 8.70 \cdot I_T − 209.15$ with $R^2 = 0.94$ (b.1). For zenith scan $L_A = 6.71 \cdot I_T − 129.84$ with $R^2 = 0.96$ (b.2). (c) L_A − leaf area (dm^2) vs. I_{3L} − impacted external leaf area (dm^2). For lateral scan $L_A = 6.40 \cdot I_{3L}$ with $R^2 = 0.97$ (c.1). For zenith scan $L_A = 3.29 \cdot I_{3L}$ with $R^2 = 0.99$ (c.2).

that using the LiDAR sensor overhead increased the number of impacts of the laser beam. Thus, the impacted areas were larger making the results of regression analysis more consistent. The question now is how to take advantage of this type of simulation, before or after using a LiDAR sensor operating in the field (LSO).

Before using the sensor in field conditions, the LSS can be used to test and optimise the main parameters of a real LiDAR operation. Among the basic parameters are the horizontal (Δy) and the angular ($\Delta \theta$) resolution of the scanning process. The data to be processed depends on these parameters, and it is advisable to reduce the acquired information while ensuring

the accuracy of the measurement. To test the effect of scanning resolution on the impacted total area (I_T), a sensitivity analysis was carried out. Table 5 shows the error that occurs when the horizontal distance between scans (Δy) increases relative to an increment of 2 mm taken as reference. The usefulness of this analysis is clear. Assuming a maximum error of 5%, the LiDAR sensor could be used by separating each scan by a distance of 20 mm.

Concerning the post-processing of a real operation with LiDAR sensor, secondary measures can be estimated using the predetermined regressions with the LSS. From data obtained from a LiDAR operation the impacted total area (IT) can be

Table 5 – An example of LiDAR simulation to study the sensitivity of the impacted total area in relation to the horizontal resolution (Δy). After the simulation, the user can compare the variation in the impacted area and the error.

Δy (mm)	I_T – impacted total area (dm^2)	$\Delta(I_T)$ (dm^2)	% Error
2	147.18	0.00	0.0%
3	147.98	0.79	0.5%
4	148.63	1.44	1.0%
5	149.26	2.08	1.4%
6	149.80	2.62	1.8%
7	149.95	2.77	1.9%
8	150.93	3.75	2.5%
10	151.93	4.74	3.2%
15	153.43	6.24	4.2%
20	154.48	7.30	5.0%
25	156.83	9.65	6.6%
35	157.43	10.24	7.0%
40	161.24	14.06	9.6%

calculated. Then, Eq. (6) can be applied to estimate L_A if the LSO has been carried out by moving laterally. Subsequent estimation of LAI is immediate if the distance between rows is also known. However, since the LSS has knowledge of the error associated with the scan resolution, overestimation of I_T can be corrected for by providing a more realistic value of L_A through the corresponding regression equation.

In short, the LSS developed in this work appears to be a reliable tool for predicting the leaf surface area of fruit trees. Furthermore, the LSS is easy to use. The program runs on a Windows operating system, and can be installed on a personal computer with a standard processor and reasonable memory capacity. The user can take advantage of this utility through subsequently developing new libraries to scan real orchards. For the moment, a snapshot of an orchard model is obtained and can be used as many times as necessary. This is especially interesting for ensuring repeatability and separate sensor–environment interaction.

4. Conclusions

A simulation program applied to fruit trees which generates an artificial orchard using a HMT model has been developed. The program simulates the growth pattern of an apple tree grown with open vase training system. Once a virtual tree is obtained, the user can simulate and predict the performance of a LiDAR system. The areas resulting from laser sensor impacts are then used to predict the tree leaf surface. The virtual tree derived by the HMT model was improved by introducing a shady index to approximate the distribution of the leaves to the experimental observations of actual tree canopies. Furthermore, this foliar correction can be applied to any training system since it does not depends on the shape of the tree. As for the LSS, the user can choose between a lateral scanning process or, instead, an overhead scanning process. Both procedures showed good prediction of the leaf area (L_A) from the impacted area (I_T). Derived from this, the program should have applications in two main fields. Firstly, the LSS is useful for laser calibration of

a real LSO. The user can compare different scanning resolutions in different scenarios allowing them to decide which the best system configuration is. The advantage in reduced time, equipment and precision is evident. Secondly, LSS is also very useful in post-processing. Data acquired in real operating conditions (LSO) can be converted to vegetative measurements using suitable regression formulae. Vegetative data that cannot be measured in a LSO could be obtained through the LSS regressions. Thus, both end users and researchers can take advantage of the optimal configuration of LS and better characterisation of scanned fruit trees.

REFERENCES

Abelson, H., & di Sessa, A. (1982). *Turtle geometry*. Cambridge: M.I.T. Press.

Arnó, J., Escolà, A., Vallès, J. M., Llorens, J., Sanz, R., Masip, J., et al. (2012). Leaf area index estimation in vineyards using a ground-based LiDAR scanner. *Precision Agriculture*. http://dx.doi.org/10.1007/s11119-012-9295-0.

Barthélémy, D., Edelin, C., & Halle, F. (1991). Canopy architecture. In A. S. Raghavendra (Ed.), *Physiology of trees* (pp. 1–19). London: J. Willey & Sons, Inc.

Bell, A. (1994). A summary of branching process in plants. In D. S. Ingram, & A. Hudson (Eds.)., *Shape and form in plants and fungi* (pp. 119–142). London: Academic Press.

Blaise, F., Barczi, J. F., Jaeger, M., Dinouard, P., & de Reffye, P. (1998). Simulation of the growth of plants. Modelling of metamorphosis and spatial interactions in architecture and development of plants. In T. L. Kunii, & A. Luciani (Eds.)., *Cyberworlds* (pp. 81–109). Tokyo: John Wiley & Sons.

Chomsky, N. (1956). Three models for the description of language. *IRE Transactions on Information Theory, 2*(3), 113–124.

Costes, E., & Guédon, Y. (2002). Modelling branching patterns on 1-year-old trunks of six apple cultivars. *Annals of Botany, 89*, 513–524.

Costes, E., Sinoquet, H., Kelner, J. J., & Godin, C. (2003). Exploring within-tree architectural development of two apple tree cultivars over 6 years. *Annals of Botany, 91*, 91–104.

Costes, E., Smith, C., Renton, M., Guédon, Y., Prusinkiewicz, P., & Godin, C. (2008). MAppleT: simulation of apple tree development using mixed stochastic and biomechanical models. *Functional Plant Biology, 35*, 936–950.

Crouse, M. S., Nowak, R. D., & Baraniuk, R. G. (1998). Wavelet-based signal processing using hidden Markov models. *IEEE Transactions on Signal Processing, 46*, 886–902.

Dauzat, J. (1993). Simulated plants and radiative transfer simulations. In C. Varlet-Grancher, R. Bonhomme, & H. Sinoquet (Eds.)., *Colloque Structure du Couvert Végétal et Climat Lumineux: méthodes de caractérisation et applications* (pp. 271–278). Saumane, France: INRA Editions.

Dauzat, J., Rapidel, B., & Berger, A. (1999). Simulation of leaf transpiration and sap flow in virtual plants: description of the model and application to a coffee plantation in Costa Rica. *Agricultural and Forest Meteorology, 109*(2), 143–160.

De Reffye, P., Elguero, E., & Costes, E. (1991). Growth units construction in trees: a stochastic approach. *Acta Biotheoretica, 39*, 325–342.

De Reffye, P., Fourcaud, T., Blaise, F., Barthélémy, D., & Houllier, F. (1997). A functional model of tree growth and tree architecture. *Silva Fennica, 31*(3), 297–311.

Delagrange, S., & Rochon, P. (2011). Reconstruction and analysis of a deciduous sapling using digital photographs or terrestrial-LiDAR technology. *Annals of Botany, 108*, 991–1000.

Diggle, A. J. (1988). ROOTMAP-A model in three-dimensional coordinates of the growth and structure of fibrous root systems. *Plant Soil, 105*, 169–178.

Durand, J. B., Gonçalvès, P., & Guédon, Y. (2004). Computational methods for hidden Markov trees – an application to wavelet trees. *IEEE Transactions on Signal Processing, 52*, 2551–2560.

Durand, J. B., Guédon, Y., Caraglio, Y., & Costes, E. (2005). Analysis of the plant architecture via tree-structured statistical models: the hidden Markov tree models. *New Phytologist, 166*, 813–825.

Ehlert, D., Heisig, M., & Adamek, R. (2010). Suitability of a laser rangefinder to characterize winter wheat. *Precision Agriculture, 11*(6), 650–663.

Escolà, A., Camp, F., Solanelles, F., Llorens, J., Planas, S., Rosell, J. R., et al. (2007). Variable dose rate sprayer prototype for tree crops based on sensor measured canopy characteristics. In: *Precision agriculture '07*. Proceedings of the 6th European conference on precision agriculture, Skiathos, Greece, 3–6 January 2007.

Fisher, J. B., & Weeks, C. L. (1985). Tree architecture of Neea Nyctaginaceae: geometry and simulation of branches and the presence of two different models. *Bull. Mus. natn. Hist. nat., Paris, ser. 4, 7, B, Adansonia.* 385–401.

Ford, E. D., Avery, A., & Ford, R. (1990). Simulation of branch growth in the Pinaceae: interactions of morphology, phenology, foliage productivity, and the requirement for structural support, on the export of carbon. *J. Theor. Biol., 146*, 15–36.

Früh, T. (1997). Simulation of water flow in the branched tree architecture. *Silva Fennica, 31*(3), 275–284.

Garrido, M., Méndez, V., Valero, C., Correa, C., Torre, A., & Barreiro, P. (2012). Online dose optimization applied on tree mass through a laser device. First RHEA International Conference on Robotics and associated High-technologies and Equipment for Agriculture. University of Pisa, September 19–21, 2012.

Gebbers, R., Ehlert, D., & Adamek, R. (2011). Rapid mapping of the leaf area index in agricultural crops. *Agronomy Journal, 103*(5), 1532–1541.

Gil, E., Escolà, A., Rosell, J. R., Planas, S., & Val, L. (2007). Variable rate application of plant protection products in vineyard using ultrasonic sensors. *Crop Protection, 26*(8), 1287–1297.

Godin, C., Guédon, Y., Costes, E., & Caraglio, Y. (1997). Measuring and analyzing plants with AMAPmod software. In M. T. Michalewicz. (Ed.), *Plants to ecosystems* (pp. 53–84). Australia: CSIRO.

Guédon, Y., Barthélémy, D., Caraglio, Y., & Costes, E. (2001). Pattern analysis in branching and axillary flowering sequences. *Journal of Theoretical Biology, 212*, 481–520.

Harper, J. L., Rosen, B. R., & White, J. (1986). *The growth and form of modular organisms*. London, UK: The Royal Society.

Holmgren, J., & Persson, A. (2004). Identifying species of individual trees using airborne laser scanner. *Remote Sensing of Environment, 90*(4), 415–423.

Lefsky, M. A., Cohen, W. B., Acker, S. A., Parker, G. G., Spies, T. A., & Harding, D. (1999). Lidar remote sensing of the canopy structure and biophysical properties of Douglas-Fir Western Hemlock forests. *Remote Sensing of Environment, 70*(3), 339–361.

Lindenmayer, A. (1968). Mathematical models for cellular interaction in development, parts I and II. *Journal of Theoretical Biology, 18*, 280–315.

Llorens, J., Gil, E., Llop, J., & Escolà, A. (2011). Ultrasonic and LiDAR sensors for electronic canopy characterization in vineyards: advances to improve pesticide application methods. *Sensors, 11*(2), 2177–2194. http://dx.doi.org/10.3390/s110202177.

Maltamo, M., Eerikäinen, K., Pitkänen, J., Hyyppä, J., & Vehmas, M. (2004). Estimation of timber volume and stem density based on scanning laser altimetry and expected tree size distribution functions. *Remote Sensing of Environment, 90*(3), 319–330.

Méndez, V., Catalán, H., Rosell, J. R., Arnó, J., Sanz, R., & Tarquis, A. (2012). SIMLiDAR – simulation of LiDAR performance in artificially simulated orchards. *Biosystems Engineering, 111*(1), 72–82.

Omasa, K., Hosoi, F., & Konishi, A. (2007). 3D lidar imaging for detecting and understanding plant responses and canopy structure. *Journal of Experimental Botany, 58*(4), 881–898.

Palacín, J., Pallejà,, T., Tresánchez, M., Sanz, R., Llorens, J., Ribes-Dasi, M., et al. (2007). Real-time tree-foliage surface estimation using a ground laser scanner. *IEEE Transactions on Instrumentation and Measurement, 56*(4), 1377–1383.

Parker, G., Harding, J., & Berger, M. (2004). A portable LiDAR system for rapid determination of forest canopy structure. *Journal of Applied Ecology, 41*(4), 755–767.

Prusinkiewicz, P., & Lindenmayer, A. (1990). *The algorithmic beauty of plants*. New York: Springer Verlag.

Riaño, D., Chuvieco, E., Condés, S., González-Matesanz, J., & Ustin, S. L. (2004). Generation of crown bulk density for Pinus sylvestris L. from lidar. *Remote Sensing of Environment, 92*(3), 345–352.

Rosell, J. R., Llorens, J., Sanz, R., Arnó, J., Ribes-Dasi, M., Masip, J., et al. (2009). Obtaining the three-dimensional structure of tree orchards from remote 2D terrestrial LiDAR scanning. *Agricultural and Forest Meteorology, 149*(9), 1505–1515.

Rosell, J. R., & Sanz, R. (2012). A review of methods and applications of the geometric characterization of tree crops in agricultural activities. *Computers and Electronics in Agriculture, 81*, 124–141. http://dx.doi.org/10.1016/j.compag.2011.09.007.

Rosell, J. R., Sanz, R., Llorens, J., Arnó, J., Escolà, A., Ribes-Dasi, M., et al. (2009). A tractor mounted scanning LiDAR for the nondestructive measurement of vegetative volume and surface area of tree-row plantations: a comparison with conventional destructive measurements. *Biosystems Engineering, 102*(2), 128–134.

Saeys, W., Lenaerts, B., Craessaerts, G., & De Baerdemaeker, J. (2009). Estimation of the crop density of small grains using LiDAR sensors. *Biosystems Engineering, 102*(1), 22–30.

Sanz, R., Llorens, J., Escolà, A., Arnó, J., Ribes-Dasi, M., Masip, J., et al. (2011). Innovative LiDAR 3D dynamic measurement system to estimate fruit-tree leaf area. *Sensors, 11*, 5769–5791.

Scala, J. J. (1988). *Análisis Vectorial. Vectores, Vol. 1*. Barcelona, Spain: Editorial Reverté, ISBN 84-291-4348-3, (In Spanish). 162–164.

Shinozaki, K., Yoda, K., Hozumi, K., & Kira, T. (1964). A quantitative analysis of plant. The Pipe model theory I. *Japanese Journal of Ecology, 14*(3), 97–105.

Sinoquet, H., Adam, B., Rivet, P., & Godin, C. (1998). Interactions between light and plant architecture in an agroforestry walnut tree. In *Agroforestry forum* (pp. 37–40).

Solanelles, F., Escolà, A., Planas, S., Rosell, J. R., Camp, F., & Gràcia, F. (2006). An electronic control system for pesticide application proportional to the canopy width of tree crops. *Biosystems Engineering, 95*(4), 473–481.

Tarquis, A., & González-Andrés, F. (1995). Stochastic L-system applied to the calculation of the leaf area of a shrubby legume for forage (Chamaecytisus rathenicus, F. ex Wol.). In M. N. Novak (Ed.), *Fractal reviews in the natural and applied sciences* (pp. 192–203). Chapman and Hall.

Tarquis, A. M., Méndez, V., Walklate, P. J., Castellanos, M. T., & Morató, M. C. (2006). L-system tree model and LiDAR simulator: estimation of spray target area. *WSEAS Transactions on Biology and Biomedicine, 3*(2), 81–88.

Tourn, G. M., Barthélémy, D., & Grosfeld, J. (1999). Una aproximación a la arquitectura vegetal: conceptos, objetivos y metodología. *Boletín de la Sociedad Argentina de Botánica, 34*, 85–99, (in Spanish).

Tumbo, S. D., Salyani, M., Whitney, J. D., Wheaton, T. A., & Miller, W. M. (2002). Investigation of laser and ultrasonic ranging sensors for measurements of citrus canopy volume. *Applied Engineering in Agriculture, 18*(3), 367–372.

Valentine, H. T. (1985). Tree-growth models: derivations employing the Pipe-model theory. *Journal of Theoretical Biology, 117*(4), 579–585.

Von Koch, H. (1905). Une méthode géométrique élémentaire pour l'étude de certaines questions de la théorie des courbes planes. *Acta Mathematica, 30*, 145–174.

Walklate, P. J., Cross, J. V., Richardson, G. M., Murray, R. A., & Baker, D. E. (2002). Comparison of different spray volume deposition models using LiDAR measurements of apple orchards. *Biosystems Engineering, 82*(3), 253–267.

Walklate, P. J., Richardson, G. M., Baker, D. B., Richards, P. A., & Cross, J. V. (1997). Short range LiDAR measurement of top fruit tree canopies for pesticide applications research in the UK. In. *Proceedings of SPIE, Vol. 3059* (pp. 143–151). Orlando, Florida: International Society for Optical Engineering Advances in Laser Remote Sensing for Terrestrial and Oceanographic Application.

Weber, J., & Penn, J. (1995). Creation and rendering of realistic trees. In *Computer graphics proceedings, annual conference series* (pp. 381–394). Acm Siggraph.

Wei, J., & Salyani, M. (2005). Development of a laser scanner for measuring tree canopy characteristics: phase 2. Foliage density measurement. *Transactions of the ASAE, 48*(4), 1595–1601.